ORIGINAL PAPER

Microseismic monitoring and deformation early warning of the underground caverns of Lianghekou hydropower station, Southwest China

Peiwei Xiao [1,2] · Tianbin Li [3] · Nuwen Xu [1,3] · Zhong Zhou [4] · Xiaohui Liu [5]

Abstract

The underground powerhouse caverns of the Lianghekou hydropower station are characterized by their depth, high geo-stress, and complicated surrounding geological conditions. To identify the excavation-induced damage zones and realize the deformation early warning of surrounding rock masses of the underground powerhouse, a high-resolution microseismic (MS) monitoring system was adopted to conduct real-time monitoring of the inner microfracture activity of the surrounding rock mass. The spatiotemporal evolution of the MS events recorded in the aggregation areas prior to the deformation of the surrounding rock mass was analyzed. The analysis results show that two typical MS event clustering zones were closely related to the blasting excavation disturbances of the omnibus bar caves and the working surfaces. The MS activity shows an obvious spatiotemporal migration evolution pattern controlled by excavation, which can be analyzed to provide some reference for future support measures. The Es/Ep value of approximately 75% of the MS events in one typical clustering zone was below 10, which indicates that the rock microfractures were dominated by non-shear failures. Furthermore, prior to the deformation relaxation of the surrounding rock mass, the MS events in the selected clustering zone increased and became rapidly concentrated, the apparent stress of the corresponding MS events suddenly decreased, and the cumulative apparent volume increased dramatically. This phenomenon of MS parameter variations can be regarded as an evaluation index of the deformation early warning of surrounding rock masses. The analysis results prove that MS monitoring is essential for the assessment and mitigation of rib spalling and collapse risks in deep underground caverns, and can be used to minimize catastrophic events involving equipment and personnel. The results of the current study may be valuable for future excavation management and safety evaluations for similar underground caverns with high in situ stresses.

Keywords Microseismic monitoring · Deformation early warning · Stability analysis · Underground cavern · Lianghekou hydropower station

Introduction

Currently, with the stable and rapid development of the society and economy of China, the demand for energy is continuously increasing. Water resources have been intensively developed and myriads of large-scale hydropower projects have been built, are being built, or are in their design and planning stages in Southwest China; these projects include Shuangjiangkou,

✉ Nuwen Xu
xunuwen@scu.edu.cn

1 State Key Laboratory of Hydraulics and Mountain River Engineering, Sichuan University, Chengdu 610065, Sichuan, People's Republic of China

2 China Energy DaDu River Hydropower Development Co., Ltd, Chengdu 610016, People's Republic of China

3 State Key Laboratory of Geo-Hazard Prevention and Geo-Environment Protection, Chengdu University of Technology, Chengdu 610059, Sichuan Province, People's Republic of China

4 PowerChina Chengdu Engineering Corporation Limited, Chengdu 610072, Sichuan, People's Republic of China

5 Key Laboratory of Fluid and Power Machinery, Ministry of Education, Xihua University, Chengdu 610039, Sichuan, People's Republic of China

Houziyan projects along the Daduhe River; the Jinping I, Ertan projects along the Yalongjiang River; and the Wudongde, Baihetan projects along the Jinshajiang River. The three large inland rivers can be seen in Fig. 1. Due to limitations in the required topography and junction layout, most of the hydropower powerhouses are arranged as underground types. Large-scale underground caverns are thus inevitably excavated and operated. For instance, the excavation dimensions of the main underground powerhouse at the Houziyan project are 219.5 m in length, 29.2 m in width, and 68.7 m in height (Xu et al. 2015). The excavation dimensions of the left bank underground powerhouse at the Baihetan project are 438.0 m × 34.0 m × 88.7 m (length × width × height, respectively) (Dai et al. 2016a). In addition, Southwest China contains the alpine and canyon region of the Hengduan Mountains of the Eastern Qinghai-Tibet Plateau. The natural geo-stress here is high and heterogeneous. The ratio of rock mass strength to geo-stress is relatively low and the geological structures are complicated. Therefore, the construction schedule and the personnel and equipment safety in those large-scale underground caverns subject to continuous excavations are seriously threatened. For example, on December 16, 2008, when the upstream sidewall of the main underground powerhouse of the Dagangshan hydropower station was excavated to the regions of the β_{80} diabase dikes (Stake mark: 0 + 132~0 + 135 m), the upstream

side of the arch collapsed, with a total volume of approximately 2968 m^3. The recovery following this serious collapse took up to 18 months (Zhang et al. 2012). Many failure phenomena such as cracks, rib spalling, unloading rebound-induced dislocations, buckling dilations, and shotcrete layer cracking occurred in the underground powerhouse of the Jinping I hydropower station subject to excavation. The relaxation depth of the surrounding rock mass was greater than 15 m, and the largest deformation was 155 mm (Li et al. 2014; Song et al. 2016). As they are affected by the complex arrangements of the numerous underground powerhouse caverns, the high in situ stress, the various lithologies and multiple geological structures, the surrounding rock mass deformation, localized spalling, and weak rockbursts were frequently experienced during the excavation of the underground powerhouse caverns of the Baihetan hydropower station (Dai et al. 2016a, b). Different degrees of deformation and failure of the surrounding rock masses occurred frequently in the underground caverns of the Houziyan hydropower station starting as early as the beginning of excavation in October 2012. In particular, the upstream sidewall of the main powerhouse deformed by approximately 100 mm in July 2013 and caused the excavation to stop for more than 2 months, which delayed construction and resulted in substantial economic losses (Xu et al. 2017). Due to the high requirements for the rock mass quality, the construction cycle and safety standards of underground
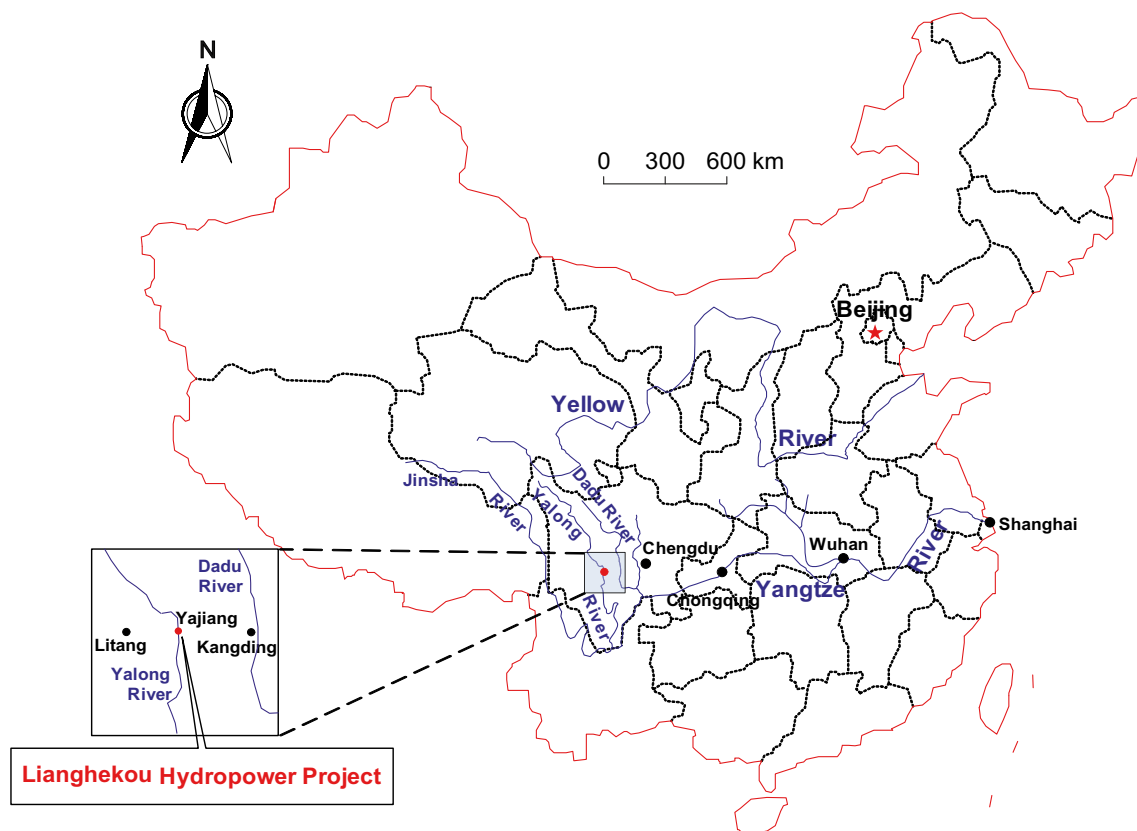

Fig. 1   Regional map of Lianghekou hydropower station

caverns as well as the complexity and difficulty of the construction procedures, the deformation prediction and safety control of the surrounding rock masses in deep underground caverns are still confronted with many technical problems and challenges. Therefore, it is of great theoretical value and practical significance to conduct an analysis and evaluation of the stability of large-scale underground caverns subject to excavation.

Distinguished from numerical simulations, physical testing, and theoretical analyses, in situ measurements are currently the most popular and direct method of monitoring the deformation of the surrounding rock mass subject to excavation. The extensive uses of measurement technologies (i.e., global positioning systems, multiple position extensometers, anchor stress gauges, convergence meters, three-dimensional laser scanner, and surface subsidence monitoring) seek to detect the surface deformations of underground caverns. These traditional monitoring methods can sufficiently reflect the stress and surface deformation characteristics of the surrounding rock masses and provide validation for numerical and physical testing results. However, these techniques cannot adequately monitor the inner microcracking of rocks, which occurs preferentially to macroscopic deformations/failures (i.e., spalling, bulking, and rockburst) of the surrounding rock masses. Thus, it is crucial to effectively capture the microfractures for analyzing and evaluating the excavation-induced risks of deep underground caverns. In fact, detectable acoustic or seismic signals are always emitted when rocks crack. If these signals can be sufficiently recorded as seismograms, the origin time, location, and source parameters of the seismic event can be obtained (Cai et al. 2001). Microseismic (MS) monitoring, a three-dimensional, real-time monitoring technique, can detect the microfracturing signals of rocks and record them as seismograms. The development and evolution trends of macrofractures can thus be deduced, and the probability of the occurrence of deformation and failure in the surrounding rock masses of underground caverns can be assessed. Over the past two decades, the MS monitoring technique has been developed into an effective approach for evaluating engineering hazards in many fields within rock slope engineering (Dai et al. 2017; Lynch et al. 2005; Ma et al. 2017; Tang et al. 2015; Xu et al. 2011, 2014) and underground cavern constructions, such as oil and gas storage (Baria et al. 2005; Ma et al. 2016), deep mines (Cao et al. 2016; Dong et al. 2016, 2018a, b; Ge 2005; Hudyma and Potvin 2010; Lu et al. 2015; Trifu and Shumila 2010; Wang 2014; Wang and Ge 2008; Young et al. 2004; Zhang et al. 2015, 2016), deep tunnels (Cai et al. 2001; Feng et al. 2015a, b, c, 2019; Hirata et al. 2007; Tang et al. 2011; Xu et al. 2016), underground powerhouses (Dai et al. 2016b; Li et al. 2017; Xu et al. 2015, 2017), and electricity generation from hot dry rocks (Tezuka and Niitsuma 2000). For example, Lynch et al. (2005) noted that the surface movements inferred from the MS data were spatially correlated with the actual surface movements of the two slope cases studied. Cao et al. (2016) revealed the MS precursory characteristics for rock burst hazard in mining areas near a large residual coal pillar in China. Hudyma and Potvin (2010) proposed an engineering approach to seismic risk management in hard rock mines. Zhang et al. (2015, 2016) demonstrated the microseismicity induced by fault activation during the fracture process of a crown pillar in the Shirengou iron mine, and the seepage channel formation using a combination of MS monitoring techniques and numerical methods for the Zhangmatun iron mine in China, respectively. Cai et al. (1998, 2001) proposed some methods of characterizing rock mass damage near excavation areas based on MS events; the quantification of rock mass damage to underground excavations could thus be realized. Xu et al. (2016) validated the applicability of the MS monitoring technique by predicting strainburst locations during the excavation of the tunnels at the Jinping II hydropower station in China. Dai et al. (2016b) conducted the deformation forecasting and stability analysis of the large-scale underground powerhouse caverns from MS monitoring. Ma et al. (2016) performed the stability analysis and deformation prediction of underground oil storage caverns by an integrated numerical and MS monitoring approach. Feng et al. (2015c) proposed a MS method for the dynamic warning of rockburst development processes in the tunnels of Jinping II project. These achievements strongly promoted the development of the MS monitoring technique as well as its use in engineering applications and our understanding of the mechanisms of rock mass failure, especially the deformation and failure forecasting of surrounding rock mass.

In the present study, the MS monitoring technique was used to realize the deformation early warning of surrounding rock mass in the deeply buried underground powerhouse caverns at the Lianghekou hydropower station, Southwest China. The geology, in situ stress characteristics, and surrounding rock mass failure phenomena of the underground caverns are briefly presented in the "Project overview" section. In the "Microseismic monitoring" section, the MS monitoring system and the temporal-spatial evolution regularities of the excavation-induced microseismicities are introduced. The focal mechanisms of the clustered MS events are also revealed. The "Deformation early warning of surrounding rock mass" section investigates the deformation early warning of the surrounding rock masses of the underground powerhouse caverns.

Project overview
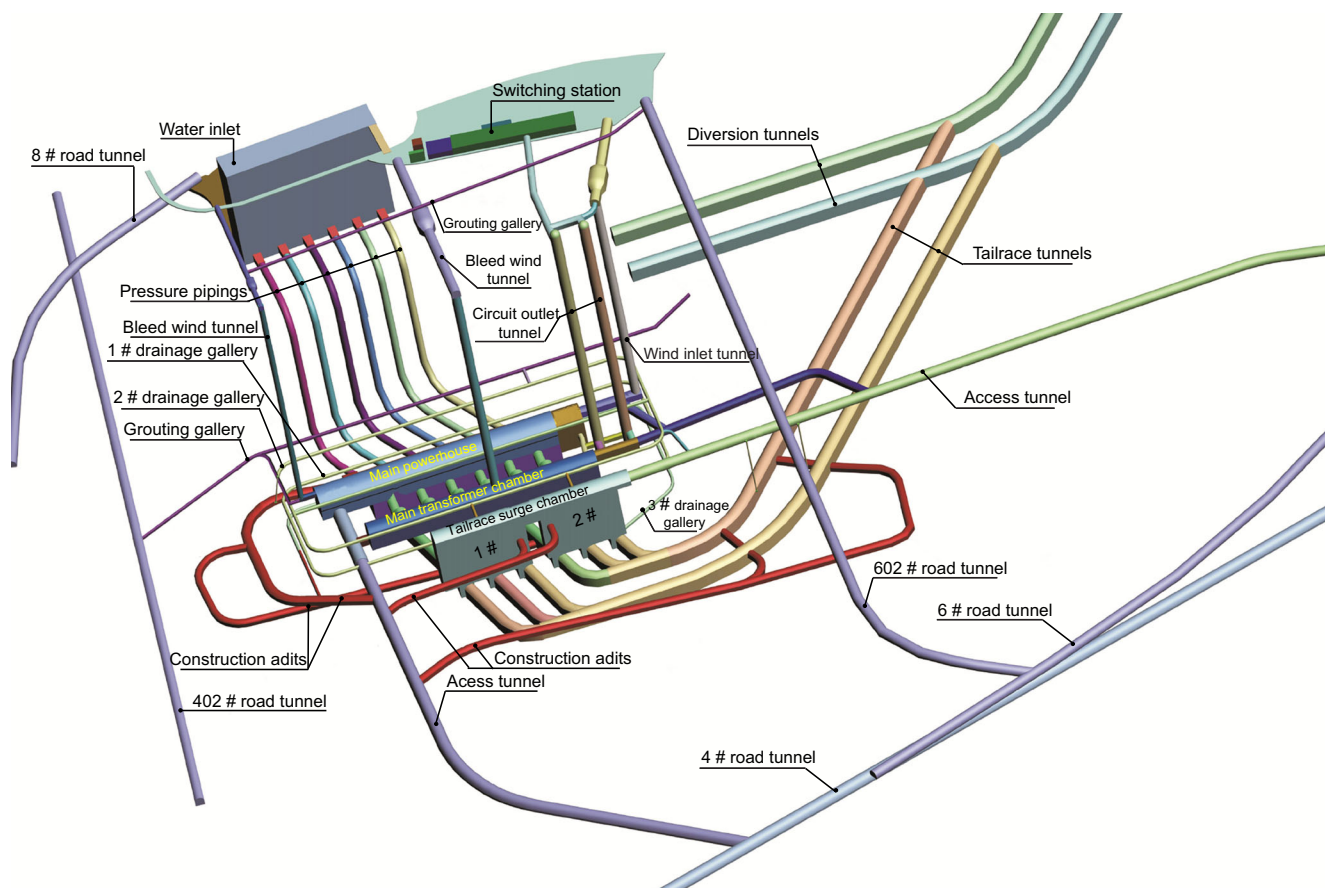
Underground caverns layout

The Lianghekou hydropower station is a large-scale step hydropower project recently constructed on the Yalongjiang River and is located in Yajiang County of the Ganzi Tibetan

Autonomous Prefecture, Sichuan province (see Fig. 1). The dam site is located approximately 2 km downstream of the intersection between the mainstream Yalongjiang and the Xianshui River tributary. The hydropower station adopts dam-type development and consists of the rock-fill dam, the right bank underground powerhouse, the left bank cavity spillways, and the discharge tunnels. The maximum height of the rock-fill dam with a gravel-soil core is 295 m. The normal water level of the reservoir is 2865 m, and the total reservoir storage is 10.767 billion cubic meters. The underground powerhouse is located in the slope of the right dam abutment, with horizontal depths of 350 to 700 m and vertical depths of 400 to 450 m. The large-scale underground powerhouse cavern group mainly includes diversion tunnels, the main powerhouse, omnibus bar caves (tunnels that connect the omnibus bars of each set to the main transformer), the main transformer chamber, the tailrace surge chamber, and tailrace tunnels. The three main caverns (the main powerhouse, the main transformer chamber, and the tailrace surge chamber) are arranged in parallel below ground along the axis direction of N3° E. Six water-turbine generator sets with 500 MW capacities per machine are installed in the main powerhouse, and the total installed capacity is 3000 MW. The excavation dimensions of the main powerhouse are 275.9 m in length, 28.4 m in width, and 66.8 m in height. The corresponding crown elevation of the main powerhouse is 2636.0 m. Thus, this underground powerhouse is one of the largest such powerhouses in China with high sidewalls and long spans. The dimensions of the main transformer chamber are 239.4 m in length, 18.8 m in width, and 25.6 m in height. The corresponding crown elevation is 2632.6 m. The dimensions of the downstream tailrace surge chambers are 190.0 m in length, 19.9 m in width, and 79.9 m in height. The horizontal distance between the centerlines of the tailrace surge chamber and the crown of the main powerhouse is 113.2 m. The thickness of the rock pillars between the main transformer chamber and the main powerhouse is 45.45 m, and the thickness of that between the main transformer chamber and the tailrace surge chamber is 45.0 m (Hou et al. 2016). The three-dimensional layout of the underground caverns at the hydropower station is shown in Fig. 2.

Geological conditions

The hydropower station is located in a mountain valley area with an asymmetric "V" shape. The slopes are characterized by sandy slate and deep valley terrains. The heights of the slopes near the valley are between 500 and 1000 m. The left bank slope is arc-shaped convex to the right bank, and its

Fig. 2 Layout of the underground cavern group at the Lianghekou hydropower station

average gradient is 55°. The right bank slope is concave with an average gradient of 45°. The geological data show that most of the rock mass of the underground powerhouse is silty metamorphic, which belongs to hard rock. The saturated uniaxial compressive strength of the rock is between 60 and 100 MPa, with an average value of 80 MPa. A small amount of the rock is silty slate, which belongs to medium hard to hard rock. The corresponding saturated uniaxial compressive strength of the rock is between 42 and 90 MPa, with an average value of 66 MPa. Due to detailed engineering geological explorations, no regional fractures occurred in the area of the powerhouse cavern. The geologic structures are characterized by bedding extrusion faults and bedding fissures (i.e., g3, g4, g6-8, g9-12, and g18-19) with a NWW strike direction. Of these faults, the fault f11 passes through the underground cavern group with a width of 0.3 to 0.5 m. The rock mass of the underground powerhouse is relatively intact, and the surrounding rock masses are generally of intermediate quality. The hydropower cavern was constructed using a conventional drill and blast method. The main powerhouse, main transformer chamber, and tailrace surge chamber were excavated using 9 benches, 3 benches, and 8 benches, respectively. A sketch of the underground powerhouse system at the elevation of 2636.0 m is shown in Fig. 3 (Hou et al. 2016). Furthermore, a stereographic projection of the faults is illustrated in Fig. 4 to allow a thorough analysis of the correlations between the faults and the underground structures.
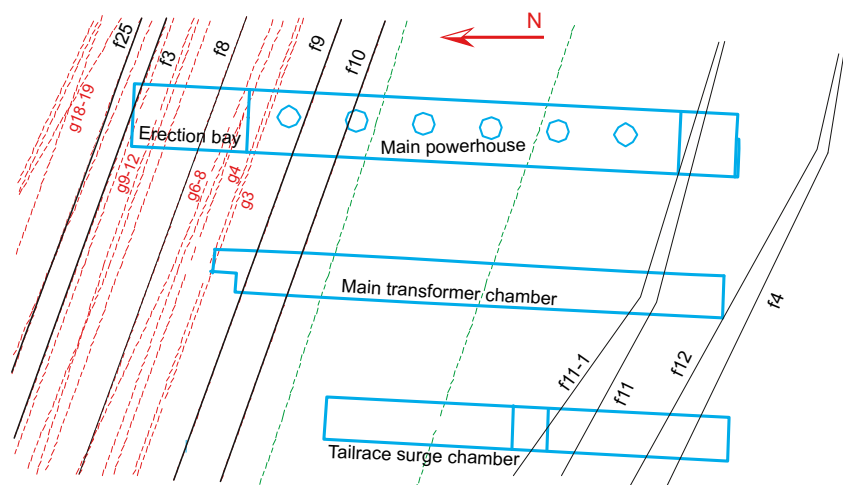
In situ stress conditions

The dam site is characterized by a deep valley and steep slopes, with heights ranging from 500 to 1000 m. The phenomena, such as rock spalling and irregular lamp-shape cake core associated with high geo-stresses, occurred in the deep exploration adits and riverbed drillings. To better understand the orientation and magnitude of the in situ stress for the design of the underground powerhouse, 7 groups of in situ

stress measurements were conducted for the right bank underground cavern group (see Fig. 5). The detailed parameters for the in situ stress measurements are presented in Table 1. The measured results show that the maximum principal stresses σ_1 in the underground cavern group are between 21.57 and 30.44 MPa, and the corresponding orientations and dip angles are between 20.3° and 57.7° and between $-2°$ and 15.6°, respectively. The intermediate principal stresses σ_2 are between 10.17 and 16.09 MPa, and the corresponding orientations and dip angles range from 245.1° to 348.5° and from $-70.8°$ to 62.3°, respectively. The minimum principal stresses σ_3 are between 5.07 and 8.78 MPa, and the corresponding orientations and dip angles range from 89.5° to 152.2° and from $-38.7°$ to 61.3°, respectively. The mean value of σ_1 is 24.77 MPa, with a relatively concentrated azimuth of N40.8° E, and the mean values of σ_2 and σ_3 are 12.36 and 6.60 Mpa, respectively. The uniaxial saturated compressive strength of the rock in the underground cavern group is between 60 and 100 MPa, and the strength-stress ratio of the rock is between 1.97 and 4.64, with a mean value of 3.23 according to the rock strength test results, which reveals that the underground cavern group belongs to a high field stress area. Figure 6a shows the high stress phenomenon (i.e., irregular lamp cake cores) occurred in the in situ stress tests of the underground powerhouse. Another high stress phenomena (i.e., splitting and rib spalling) occurred early in the excavation process in areas near the underground powerhouse arch-crown is shown in Fig. 6b.
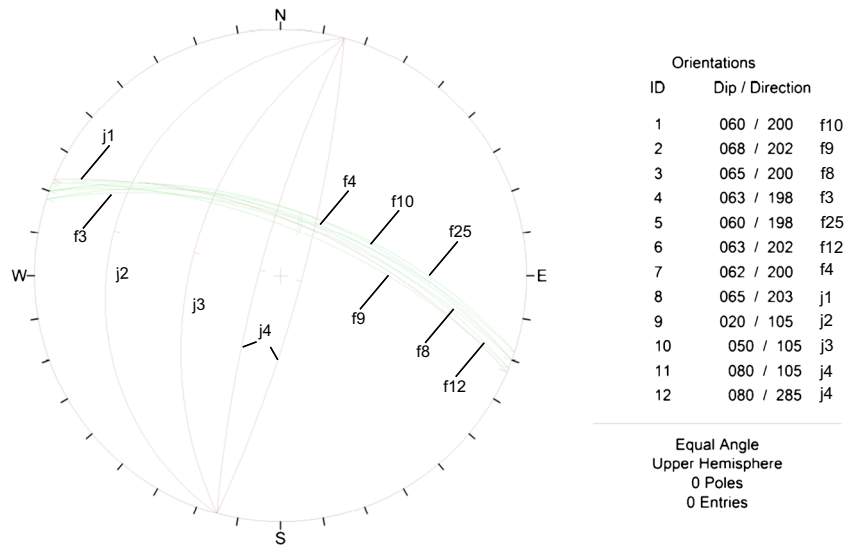
Deformation failure characteristics of surrounding rock masses subject to excavation

Large-scale rock mass instabilities and failures did not occur during the excavation processes of the underground cavern group. The surrounding rock mass of the underground powerhouse is relatively stable. However, the stability of some local surrounding rock masses controlled by fractures is poor, which is characterized by splitting, rib spalling (Fig. 7a, b) and

Fig. 3 Sketch of underground powerhouse system at elevation of 2636.0 m

Fig.4 A stereographic projection of the faults in the underground cavern group

Orientations		
ID	Dip / Direction	
1	060 / 200	f10
2	068 / 202	f9
3	065 / 200	f8
4	063 / 198	f3
5	060 / 198	f25
6	063 / 202	f12
7	062 / 200	f4
8	065 / 203	j1
9	020 / 105	j2
10	050 / 105	j3
11	080 / 105	j4
12	080 / 285	j4

Equal Angle
Upper Hemisphere
0 Poles
0 Entries

shallow unstable blocks in the fracture zones (Fig. 7c, d). According to the field observations, the surrounding rock mass failures usually occurred after excavations or in the process of cleaning the surfaces of the excavated rock mass, whether or not the splitting and spalling or block slip features were present. The corresponding damage depths usually range from 0.5 to 2.0 m. The phenomena of local surrounding rock mass failure can be interpreted as an excavation-induced unloading of shallow rock strata. Notably, the shallow rock strata are all controlled by the system anchor bolts in the effective anchorage range. Furthermore, the support design parameters of the anchor bolts are optimized in the critical sections of the local fractures in the light of the actual geological conditions after the excavation.

Microseismic monitoring

Description of MS monitoring

To real time monitor and analyze the characteristics of microfractures in the surrounding rock mass of the underground caverns in the Lianghekou hydropower station subject to continuous excavation, a high-resolution MS monitoring

Fig. 5 Distribution diagram of the in situ stress measurement points at the underground cavern group of the Lianghekou hydropower station
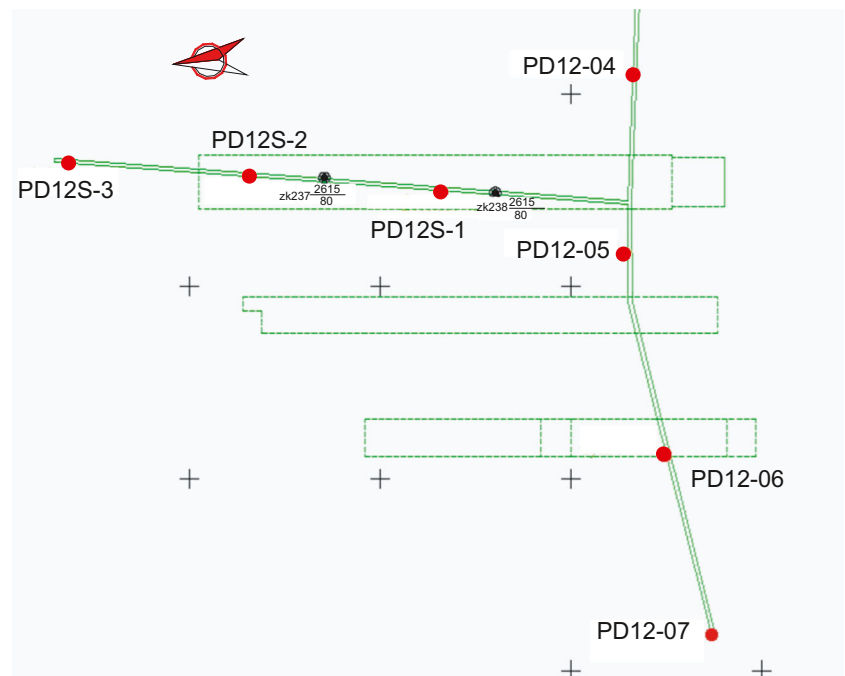
Table 1 The results of rock mass in situ stress measurements in the geological exploration tunnels

| No.	Measuring points	Measuring point locations	Elevation/m	Horizontal depth/m	Vertical depth/m	Lithology		σ_1	σ_2	σ_3
1	σ_{PD12-4}	PD12 0+400 m	2616	400	370	Silty metamorphic	Value (MPa)	21.6	10.2	5.7
							α (°)	20.3	293.7	109.2
							β (°)	−2.0	60.6	29.3
2	σ_{PD12-5}	PD12 0+494 m	2616	494	458	Silty metamorphic	Value (MPa)	23.6	13.4	7.50
							α (°)	51.0	328.0	89.5
							β (°)	−23.2	16.0	61.3
3	σ_{PD12-6}	PD12 0+600 m	2616	600	556	Silty metamorphic	Value (MPa)	24.6	12.4	7.6
							α (°)	43.3	322.8	119.2
							β (°)	−11.8	38.3	49.3
4	σ_{PD12-7}	PD12 0+700 m	2616	700	650	Silty metamorphic	Value (MPa)	23.9	12.0	8.8
							α (°)	57.7	348.5	137.0
							β (°)	15.6	−51.9	−33.8
5	$\sigma_{PD12S-1}$	PD12S 0+98 m	2616	488	447	Silty metamorphic	Value (MPa)	25.2	10.3	5.6
							α (°)	43.0	245.1	134.9
							β (°)	−17.9	−70.8	−6.8
6	$\sigma_{PD12S-2}$	PD12S 0+200 m	2616	506	423	Silty metamorphic	Value (MPa)	24.1	16.1	5.9
							α (°)	34.7	342.1	152.2
							β (°)	−17.7	62.3	20.6
7	$\sigma_{PD12S-3}$	PD12S 0+294 m	2616	530	440	Silty metamorphic	Value (MPa)	30.4	12.1	5.07
							α (°)	35.5	293.0	135.8
							β (°)	−10.6	−49.3	−38.7

α is the angle of the principal stress in the horizontal projection. The angle of true north is zero and clockwise rotation. While β is the dip angle of the principal stress and the angle of elevation is positive
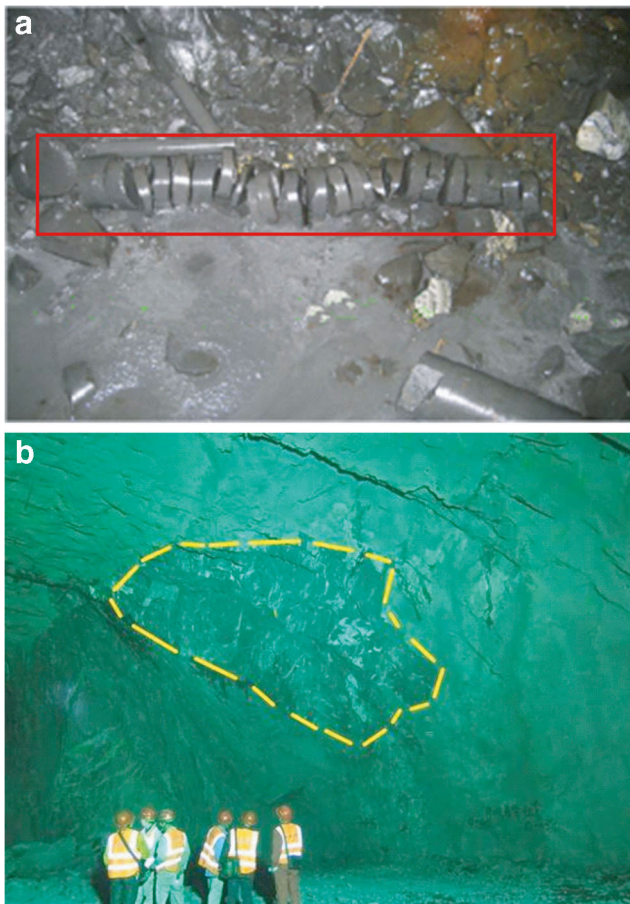
Fig. 6 The high stress phenomena in the underground powerhouse. **a** The irregular lamps cake core and **b** rock mass splitting and spalling occurred at the upstream arch springing of the assembly bay in the underground powerhouse

system manufactured by ESG (Engineering Seismology Group, Canada) was installed in the underground cavern group. The monitoring system consists of a Hyperion digital signal processing system, a Paladin digital signal acquisition system, and 12-channel uniaxial accelerometers (9 of them were installed in the first layer of drainage gallery, 3 of them were installed in the different omnibus bar caves, and another 6 will be supplemented dynamically in the later excavation, as shown in Fig. 8). The accelerometers which have a frequency response from 50 Hz to 5 kHz ($\pm$ 3 dB) were grouted at the end of diamond-drilled boreholes in the sidewalls of the service tunnels. The 12-channel seismic monitoring system can cover the crown, upstream, and downstream zones of the main powerhouse and the middle wall between the main powerhouse and main transformer chamber. The sensor array located at different elevations can be used to monitor excavation-induced microfracturing in real time. Nine uniaxial accelerometers were placed in the first layer of the drainage tunnels, which are located at the upstream and downstream of the main powerhouse, and at the upstream of tailrace surge chamber, respectively. Other sensors were distributed in the rock mass between the main powerhouse and main transformer chamber. Due to geological limitations in the underground caverns, no GPS signal can be used as a time source; therefore, the Paladin units rely on a pulse per second signal from the Paladin Timing Source over the network. This method allows the data from each Paladin to be accurately timestamped, to ensure that multiple units are synchronized (Urbancic and Trifu 2000; Xu et al. 2011). Furthermore, on-site fixed point blasting tests and sensor tap tests were performed to verify the positioning accuracy of the seismic monitoring system. The seismic source

Fig. 7 Scene photos of the surrounding rock mass failures in the underground powerhouse. **a** Spalling occurred at the upstream arch-crown (stake no. 0 + 55–0 + 65 m), **b** splitting and spalling occurred at the upstream arch-crown (stake no. 0 + 77–0 + 85 m), **c** unstable blocks controlled by adverse structural planes in the arch-crown, and **d** exposure of fractures development after the pilot tunnel excavation
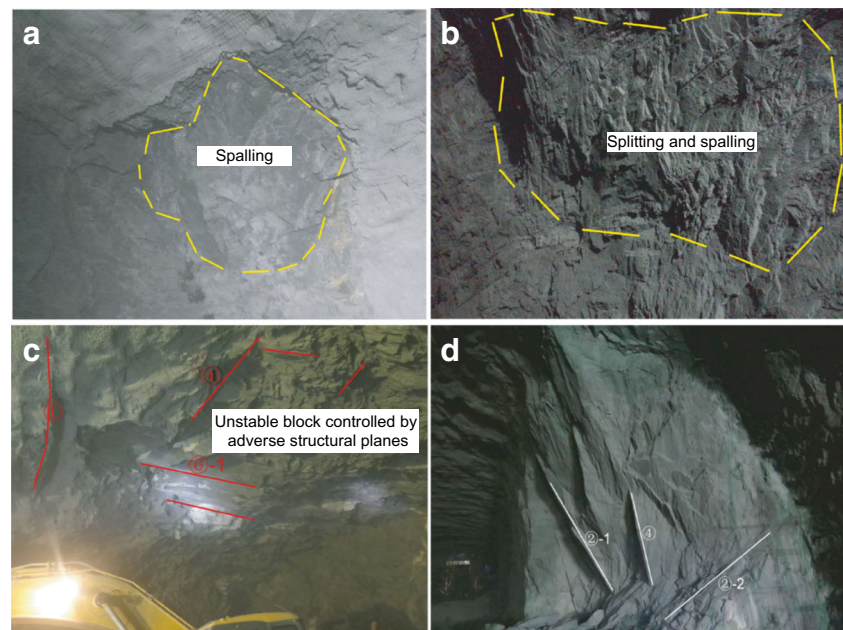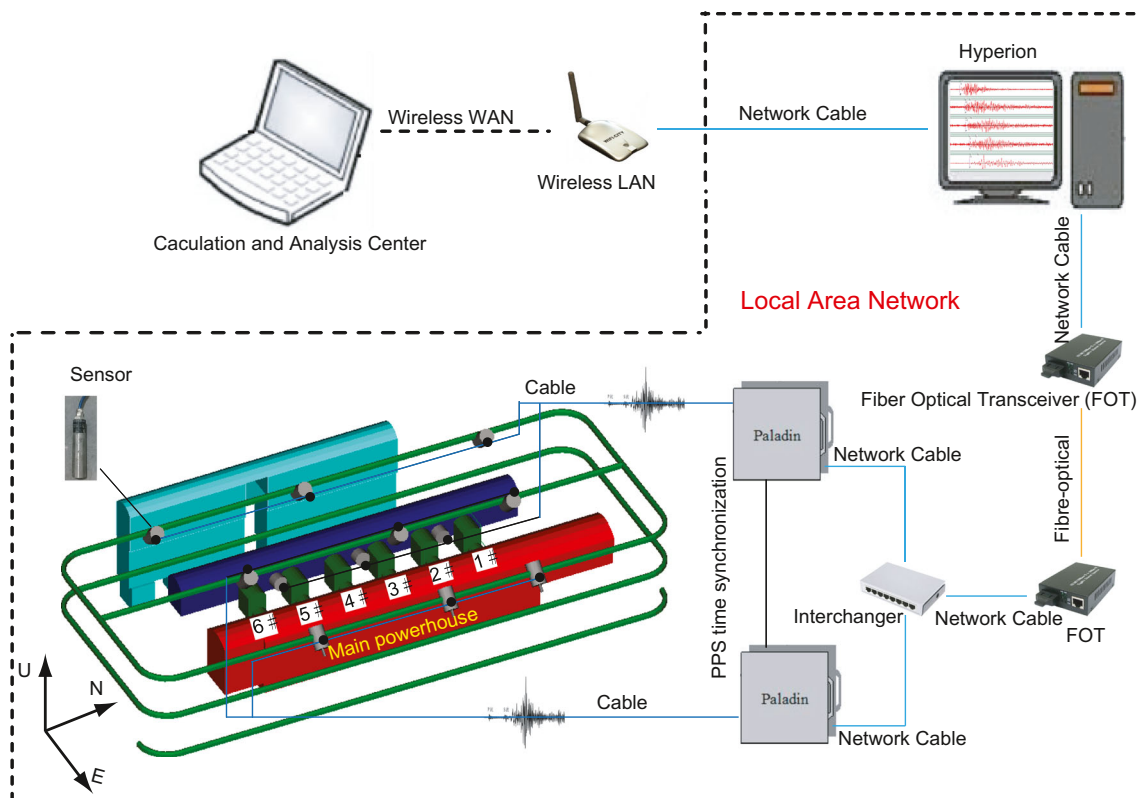
Fig. 8 Network topology of MS monitoring system

location error was less than 5 m in the scope of the sensor array when manual processing was used.

The Hyperion processing system was used to digitize the seismic data with a sampling frequency of 10 kHz and was used to perform preliminary event detection when the recorded signals of the substations exceed a given threshold using the short time average vs. long time average algorithm (STA/LTA). Constant P- and S-wave velocities were initially estimated from a joint investigation of on-site blasting tests and digital sound wave tests. The calibrated results indicate that Vp = 4600 m/s and Vs = 2656 m/s. More details can be found in the related literatures (Trifu and Shumila 2010; Urbancic and Trifu 2000; Xu et al. 2011).

## Spatial distribution characteristics of MS events

The microfracture activities of the surrounding rock masses are closely associated with construction conditions. Figure 9 shows the spatial distribution of the MS events that occurred in the crown areas of the main powerhouse and the main transformer chamber during the selected period of April 12 to May 14, 2016. It was found that the magnitudes of the MS events are small, ranging from − 1.8 to − 0.8. Most of these events are distributed in the middle pillar wall between the main powerhouse and the main transformer chamber (with elevations ranging from 2618 to 2670 m). Two concentrated zones are located at the crown regions between the 5# and 6#

omnibus bar caves (namely, zone "I") and the crown regions between the 3# and 4# omnibus bar caves (namely, zone "II"). The MS event concentration phenomena can be interpreted as follows: the initial stress equilibrium state was disturbed due to an excavation-induced unloading of the surrounding rock mass. Then, the adjustment and redistribution of the internal stress states contributed to the phenomena of stress concentration and energy aggregation in local regions. When the stress concentrations and energy aggregation reached a certain degree, rock microfractures occurred, as did energy release, and new stress equilibrium was formed. Combined with the field construction analysis, the MS concentration zones "I" and "II" were closely associated with the excavation-induced unloading of the omnibus bar caves in the selected period.

The excavation on the upstream side of the III$_1$ layer of the main powerhouse and the tests of the bearing capacity of the rock anchor beams were conducted during the selected monitoring period. There were still small amounts of microfracture activities, although the overall excavation strength was weak. Moreover, a small number of microfractures also occurred in the surrounding rock mass of the crown area between the assembly bay characterized by the developed compression faults and bedding fissures and the 1# unit subjected to excavation disturbance in the lower sidewalls. However, no obvious aggregation phenomenon appeared in the region.

The energy release from MS events is an important criterion for determining the degree of damage of the surrounding

Fig. 9 Spatial distribution of MS events. **a** Top view and **b** front view
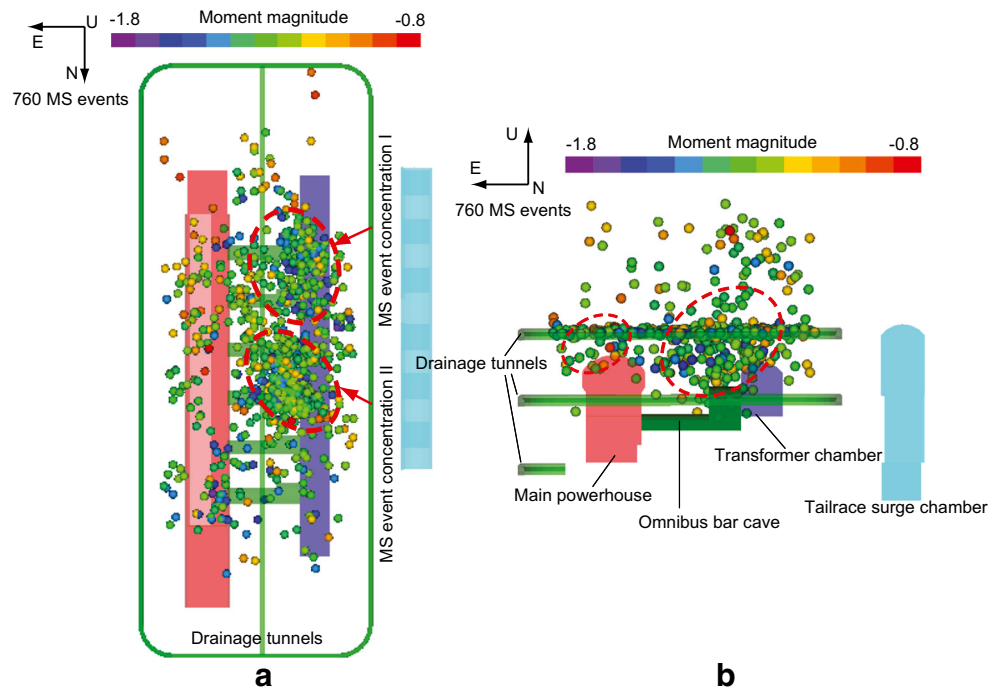
rock mass (Lu et al. 2015). Figure 10 shows an energy release density contour of the MS events that occurred during the selected monitoring period. It can be found that the regions with intense energy release were mainly distributed near the upstream sidewall of the main transformer chamber between the 3# and 4# omnibus bar caves (namely, "a"), and the crown area of the main transformer chamber between the 5# and 6# omnibus bar caves (namely, "b"), respectively, which

coincides with the spatial distribution of the MS events shown in Fig. 9. Herein, besides the excavation patterns, the energy release of the surrounding rock mass damage mainly depends on the initial stress field of the surrounding rock mass before damage and the geological conditions of the surrounding rock mass. According to the geological exposure obtained at the elevation of 2636 m of the main powerhouse as shown in Fig. 2, the steep dip bedding extrusion faults f11 and f11-1 passed

Fig. 10 Energy release density contour of MS events
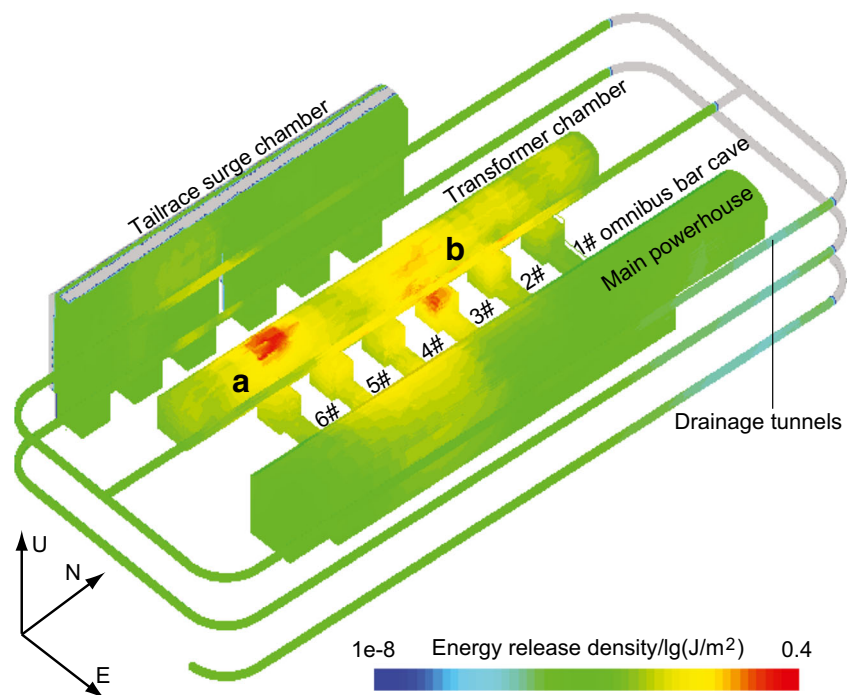
through the crown region of the main transformer chamber between the 5# and 6# omnibus bar caves, which might contribute to the intense energy release of the MS events.

Spatiotemporal evolution of MS event migration

The aggregation of MS events that occurred in the underground cavern group is attributed to multiple factors, such as excavation intensity and scale, cavity structure arrangement, and in situ stress state (Dai et al. 2016b). To reveal the dominant causal factor of microfractures that occurred in the main

powerhouse, the spatiotemporal evolution of the MS event migrations of the two clustering zones mentioned above is investigated in this section. Some references are thus used for monitoring and early warning of engineering constructions.

Figure 11 shows a map of the stratified excavation of the underground powerhouse caverns. Excavations of the bottom of layer II_2 in the main transformer chamber and the large sections (layer I) of the 3#, 4#, 5#, and 6# omnibus bar caves were conducted during the selected monitoring period. The horizontal and vertical cross free surfaces of the upstream

Fig. 11 The sketch map of the stratified excavation in the underground powerhouse caverns. **a** Cross section of 5# omnibus bar cave, **b** three-dimensional excavation progress, **c** on-site photo of main transformer chamber after excavation, and **d** on-site photo of the main powerhouse after excavation
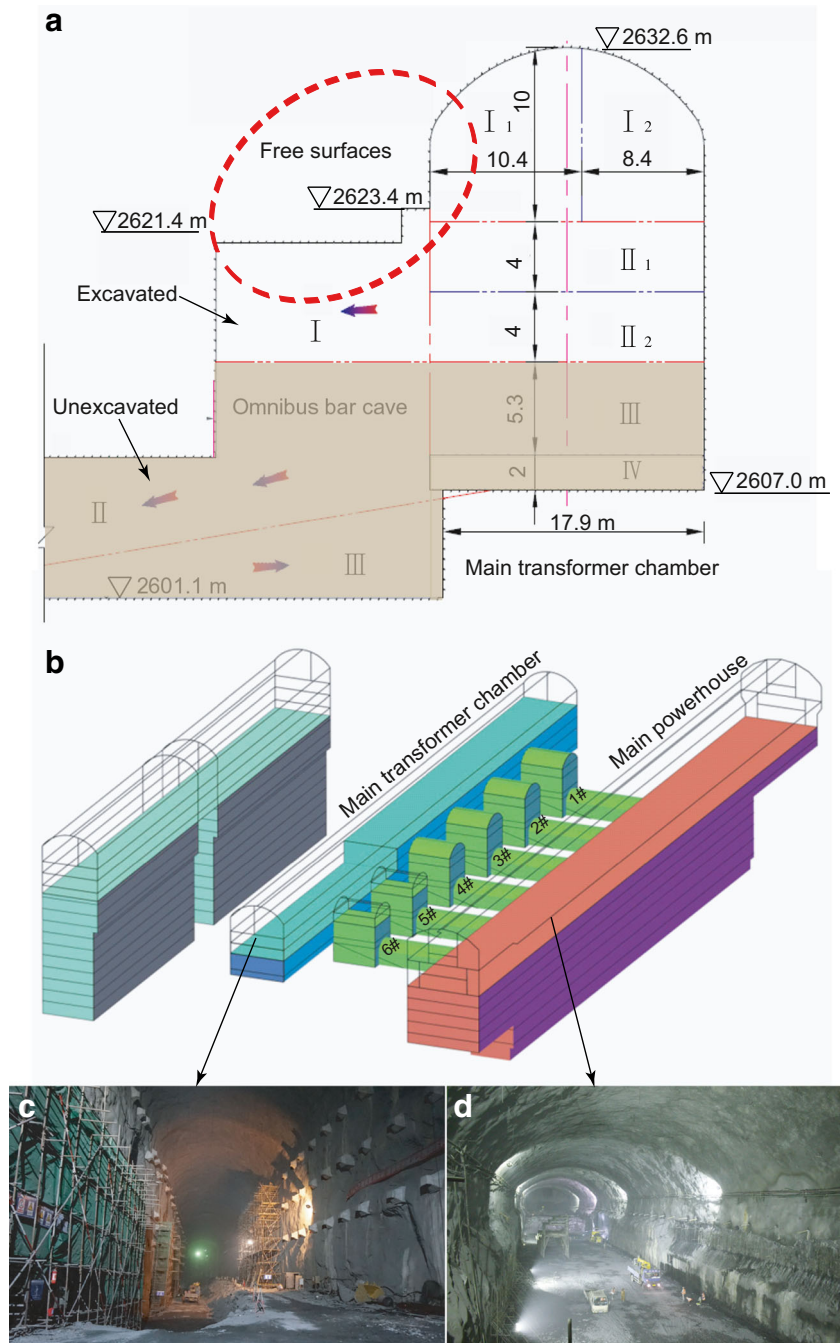
sidewalls of the main transformer chamber were gradually formed. The microfractures occurred in the surrounding rock mass showed obvious spatiotemporal migration characteristics subject to excavation unloading.

Figure 12 shows the spatiotemporal migration pattern of the MS events that occurred in the upstream sidewalls of the main transformer chamber, which was subject to continuous excavation. These two aggregated areas "I" and "II" were delineated and their corresponding spatiotemporal distributions of the MS events were investigated. As seen in Fig. 12a, most of the MS events in the aggregated area "I" occurred between April 25 and 29, 2016, with an average rate of approximately 25 per day. The peak rate of the MS events was 36, which occurred on April 28, 2016. The majority of the

MS events in the aggregated area "II" occurred between May 6 and 11, 2016, with an average rate of approximately 27 per day. The peak rate of the MS events was 48, which occurred on May 11, 2016. The MS activities that occurred in these two aggregated areas during the rest of selected monitoring period were comparably weak, with an average rate of approximately 5 per day. Figure 12b shows the spatial distribution of the MS event concentrations. Herein, the spheres represent MS events, the colors represent different moment magnitudes, and the scales denote the different energy releases of MS events. The aggregated area "I" is located at the crown region between the 5# and 6# omnibus bar caves, with elevations ranging from 2615 to 2660 m, and the corresponding moment magnitudes ranging from -1.0 and -1.6. The

Fig. 12 The temporal and spatial evolution of MS activity in the surrounding rock mass of the upstream sidewall in main transformer chamber. **a** Temporal distribution of MS events, **b** spatial distribution of MS events, **c** on-site photo of 5# and 6# omnibus bar caves excavation, and **d** on-site photo of 3# omnibus bar cave excavation
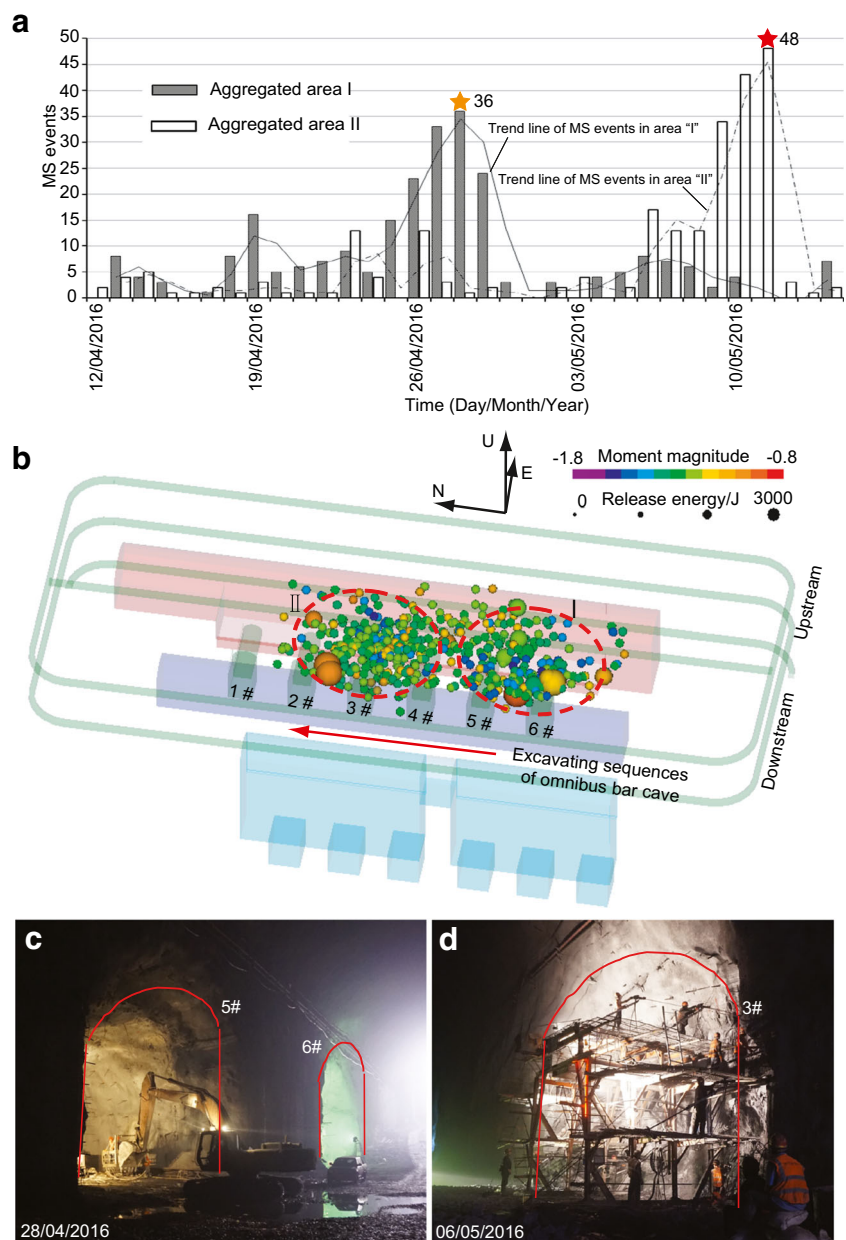
aggregated area "II" is located at the crown region between the 3# and 4# omnibus bar caves, with the elevations ranging from 2615 to 2650 m, and the corresponding moment magnitudes ranging from −0.9 to −1.5. The MS events that occurred in both of these two aggregated areas are characterized by their small magnitudes and high activity rates. It is worth noting that the magnitudes and energy releases of the MS events that occurred in the aggregated area "I" are greater than those that occurred in the aggregated area "II." According to the geological data and field observations, the phenomenon can be interpreted as bedding extrusion faults f11 and f11-1 passing through the surrounding rock mass adjacent to the aggregated area "I." This stress concentration phenomenon occurring in weak structural planes would be more obvious.

Essentially, MS activity is the external manifestation of site-construction (i.e., blasting excavation) induced stress disturbances and damages of the surrounding rock mass. According to the construction schedule, the blasting excavations of the six omnibus bar caves adjacent to the main transform chamber have been conducted since April 23, 2016. The on-site blasting excavation photos of the 5# and 6# omnibus bar caves during the period between April 24 and 28, 2016, and those of the 4# and 3# omnibus bar caves during the period between May 6 and 11, 2016, are shown in Fig. 12c, d, respectively. The original cracks in the surrounding rock masses in the study of interest were activated and expanded to damage subject to the combined effects of the explosive shock waves and detonation gases with high temperatures and pressures during the blasting excavation period. After excavation, the surrounding rock masses of the crowns of the omnibus bar caves formed free surfaces in the horizontal and vertical directions, which resulted in a sharp adjustment of the stress. The initiation, propagation, and coalescence of the microcracks of the deep rock masses were thus conducted during the energy release processes. Consequently, there was obvious spatiotemporal migration regularity in the MS activity for areas subject to excavation disturbances. According to this regularity, the occurrence, extension, and migration of the interior damages of the surrounding rock masses can be dynamically identified in real time, and the excavation-induced damage zones can thus be delineated.

Focal mechanism of MS events in the aggregated area "I"

MS event releases energy in the form of P and S waves, as well as via seismic waves the P and S waves can be captured and located by the sensors in the study area. Some previous studies (Boatwright and Fletcher 1984; Gibowicz et al. 1991; Hudyma and Potvin 2010; Dai et al. 2016a, b) have proved that the ratio of S-wave to P-wave energies (Es/Ep) can be used to analyze the focal mechanisms of MS events. It has been found that for fault-slip type events, there is significantly

more energy in the S wave than in the P wave (Boatwright and Fletcher 1984). Frequently, the ratio of S-wave energy to P-wave energy is greater than 10 (Cichowicz et al. 1988). Similarly, Duplancic (2002) found that shear-related caving events had high ratios of S-wave to P-wave energies. For non-shear type event mechanisms, such as strain-bursting, tensile, and volumetric stress change seismic events, there is relatively more P-wave energy (Urbancic et al. 1992), with a ratio of S-wave to P-wave energies that is frequently in the range of 1 to 3. Therefore, the ratio of S-wave to P-wave energies is strongly related to the seismic event mechanism (Gibowicz et al. 1991; Urbancic et al. 1992).

Figure 13 shows the distribution curve of the ratio of S-wave to P-wave energies in the aggregated area "I." The ratio of S-wave to P-wave energies for approximately 75% of the MS events is less than 10. This result can be interpreted as the surrounding rock mass damage being characterized by non-shear type failures, accompanied by a small number of shear failures. Figure 14 shows the excavation exposure surface of the large cross section of the 5# omnibus bar cave (with a length of 10 m and height of 7 m). It can be found that the rock mass integrity after its excavation was fairly good. However, some tensile fractures and spalling of the surrounding rock mass occurred at the arch of the 5# omnibus bar cave (see Fig. 14c), and these failure phenomena were attributed to the stress adjustment of the excavation-induced vertical unloading. Furthermore, spalling of the surrounding rock mass also occurred at the arch springing after excavation, as shown in Fig. 14b. Such non-shear type failures of the surrounding rock masses validated the analysis results of the focal mechanism of the MS events occurred in the aggregated area "I."
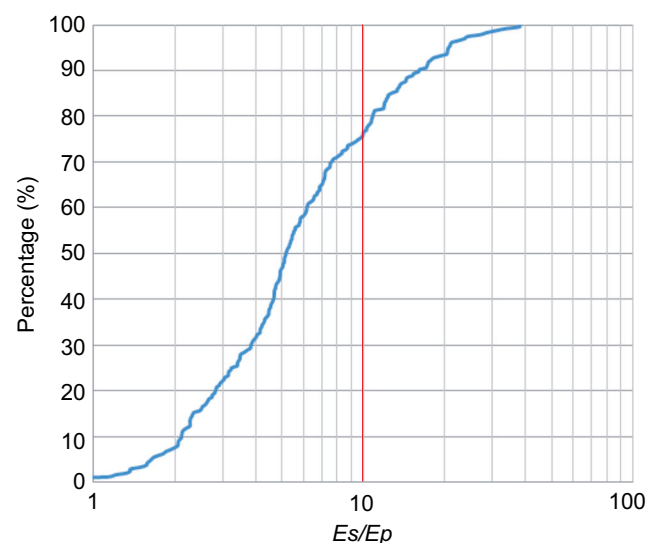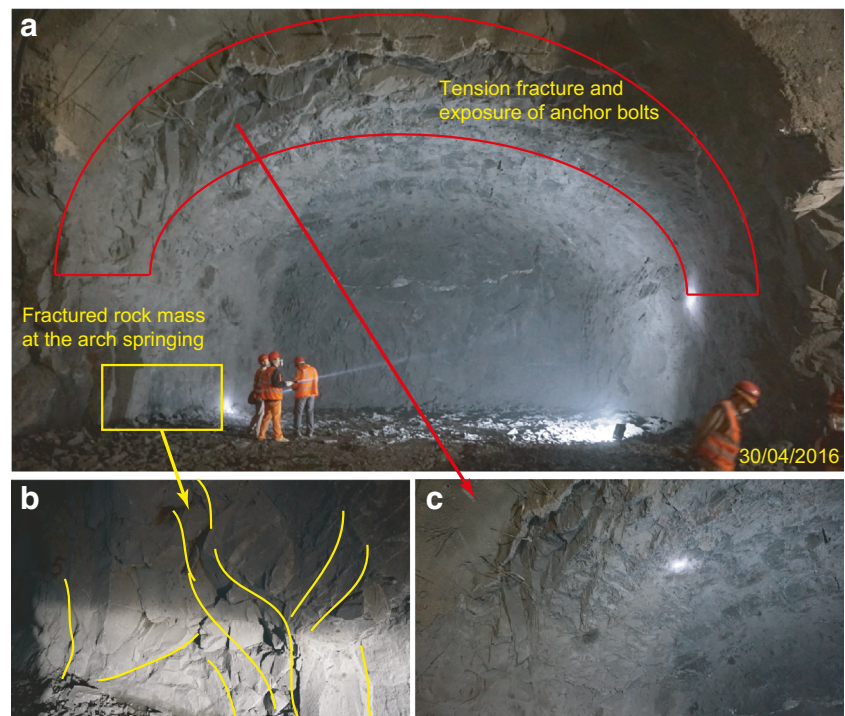

Fig. 13 The percentile curve of Es/Ep for MS events in the clustering zone I

**Fig. 14** Excavation completion
photograph of 5# omnibus bar
cave

## Deformation early warning of surrounding rock mass

During the monitoring period, the anchor stress gauges Rr-5ZB-4 and Rr-6ZB-1 were installed in the upside arches of omnibus bar caves 5# and 6# at the upstream sidewall of the transformer chamber, as shown Fig. 15a. Figure 15a shows the stress process curves of the anchor stress gauges and the temporal distributions of the MS events between April 1 and May 7, 2016. It can be found that the anchor stress gauges showed no obvious changes between April 1 and 27, 2016. Sharp increases were observed at the anchor stress gauges Rr-5ZB-4 and Rr-6ZB-1 since April 27, 2016. The value of the "2 m" point of the anchor stress gauge Rr-5ZB-4 was 123.68 MPa and the value of the "4 m" point of the anchor stress gauge Rr-6ZB-1 was 77.90 MPa on May 6, 2016. Combined with the temporal and spatial distributions of the MS events in Fig. 15a, b, it can be found that the average number of MS events was 5 per day. However, MS activity occurred frequently, at an average rate of 25 events per day between April 25 and 29, 2016. In particular, the number of MS events reached 36 on April 28, 2016. The majority of the MS events were concentrated near the anchor stress gauges (see Fig. 15b). The sudden increase of MS events and their concentrations indicated that the damage of the interior rock mass had increased and the deformation and relaxation of the surrounding rock mass had occurred. This change can explain the rapid growth phenomenon at the two anchor stress gauges starting on April 27, 2016. Furthermore, this explanation shows that the deformation and failure of the surrounding rock

mass usually lags behind the changes of the temporal-spatial distributions of the MS event concentrations. Therefore, the pattern of the initiation, coalescence, expansion, and accumulation of MS events can be regarded as precursors of the deformation and damage of the deep surrounding rock mass.

Statistical analyses of the spatiotemporal evolutionary patterns of the MS events have been widely used to estimate the underground rock mass stability (Dai et al. 2016b; Lu et al. 2015; Zhang et al. 2015). From a seismological perspective, the apparent stress and apparent volume are two significant parameters used to describe the variation characteristics of the rock mass damage before and after seismicity. The related calculation equations were illustrated in Dai et al. (2016b) in detail. Here, Fig. 16 shows the variation pattern of the apparent stress and apparent volume before and after the deformation of the surrounding rock mass in the aggregated area "I." Before April 21, 2016, the values of the apparent stress and cumulative apparent volume were small, but both had slow growth trends. At this time, the excavation of the large cross-sectional openings of 5# and 6# omnibus bar caves started, which resulted in weak unloading disturbances and a small number of surrounding rock mass ruptures. The apparent stress increased rapidly and the cumulative apparent volume was still in a slow growth stage during the period between April 22 and 24, 2016. At this time, the excavation progresses of the omnibus bar caves 5# and 6# continued and the surrounding rock mass stress were sharply adjusted, which contributed to the obvious aggregation phenomenon of the MS events, as shown in Fig. 12b. However, the apparent stress dropped suddenly and the cumulative apparent volume
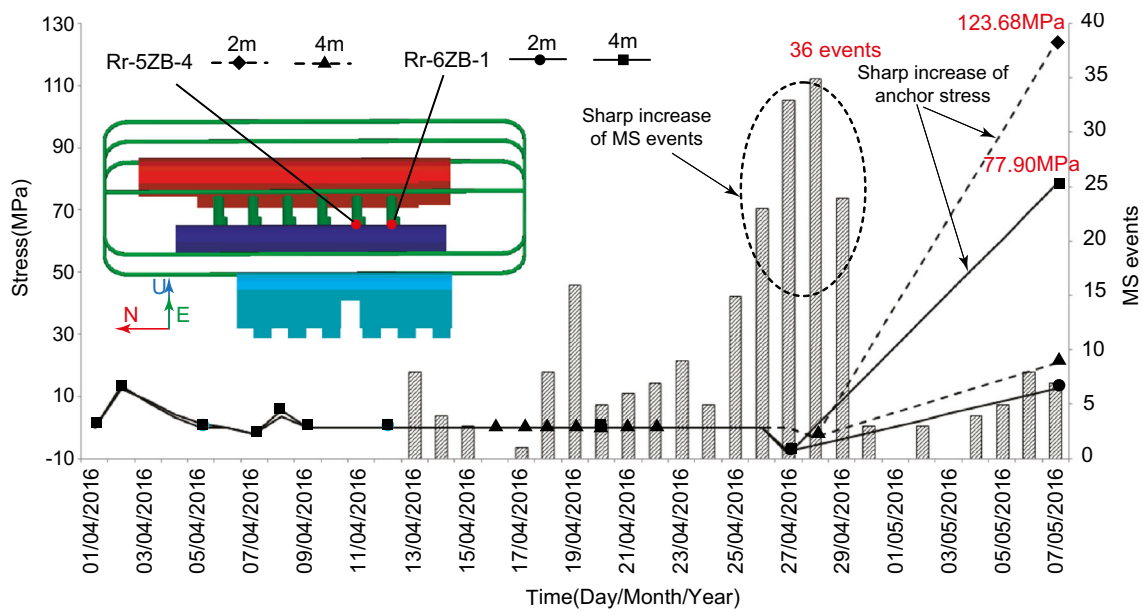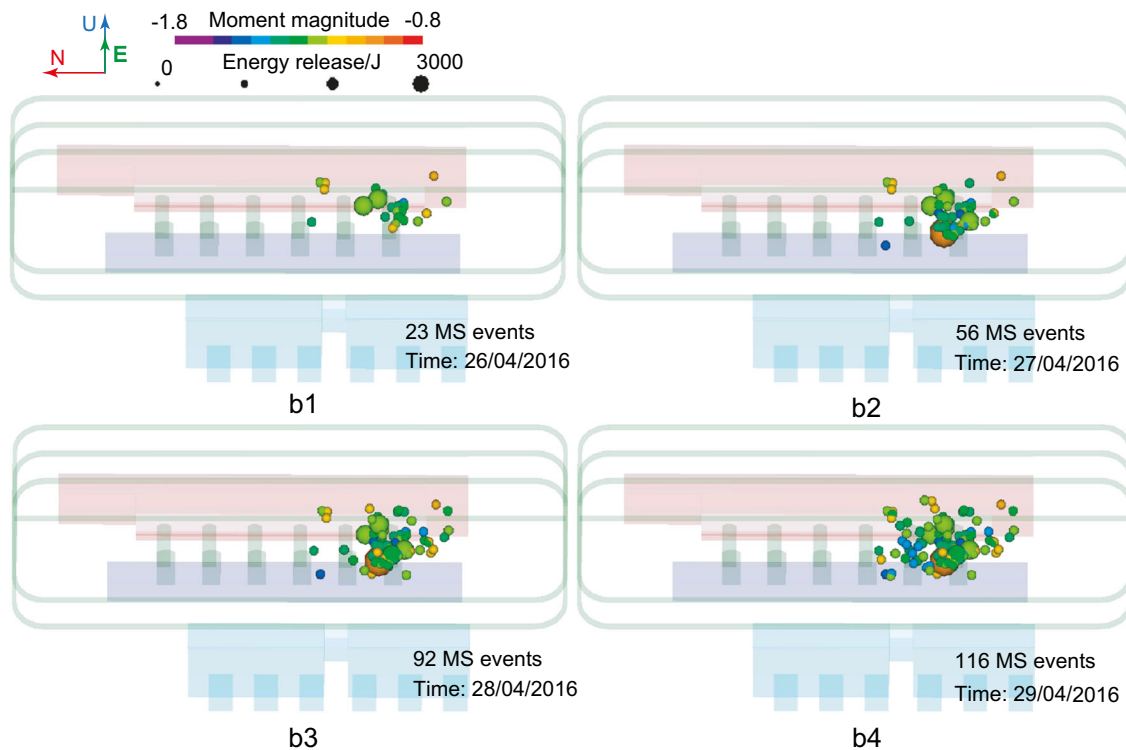
Fig. 15 Comparison between rock mass deformation and temporal and spatial evolutionary characteristics of MS events. **a** The correlation between MS activity and anchor stress variations and **b** spatial distribution of MS event accumulations

presented a significantly increase trend during the period between April 24 and 27, 2016. This period can be regarded as the early warning period for the surrounding rock mass deformation according to the statements above (Dai et al. 2016b). There were sharp increases at the anchor stress gauges Rr-5ZB-4 and Rr-6ZB-1 installed in the aggregated area "I" since

April 27, 2016, as shown in Fig. 15a. From this phenomenon, it can be inferred that the surrounding rock mass deformed towards the freeing surfaces after excavation unloading, therefore leading to the tension of anchor bolts.

As we know, the strain and stress of the rock increase before the applied load reaches its peak stress. This period

Fig. 16 Variation pattern of apparent stress and cumulative apparent volume of MS events occurred in the aggregated area "I"
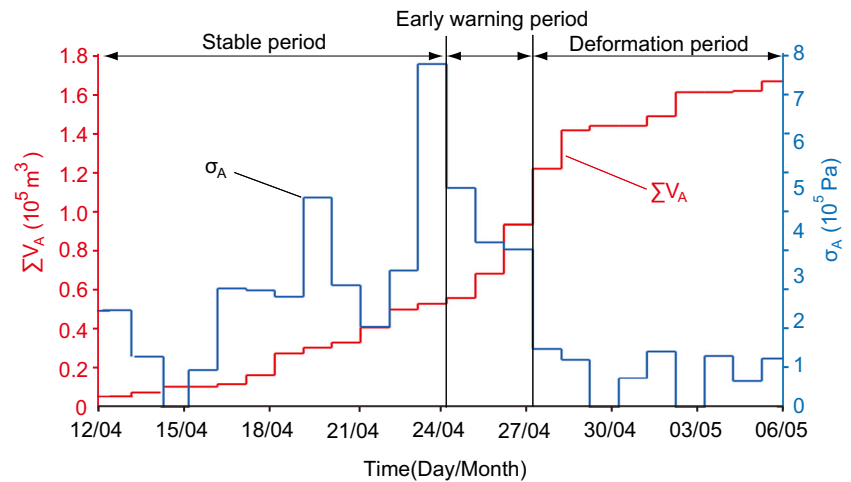
belongs to the stage of strain hardening, and the medium is stable; the strain increases and the stress decreases sharply after the applied load exceeds the peak stress. This period belongs to the stage of strain softening, and the medium is unstable (Martin and Chandler 1994; Hoek and Martin 2014). The same phenomena were found in the processes of surrounding rock mass stress and strain variation during the occurrence of rockbursts in a coal mine (Zhang 1987) and during excavation-induced fault activation in an iron mine (Zhang et al. 2015). Similarly, combined with the MS activity rate, the relationship between the MS activity characteristics and the surrounding rock mass deformation of the underground caverns can be obtained after analyzing the characterization of the variation of the apparent stress and apparent volume of the aggregated area "I" after the excavation. Namely, when the MS events are concentrated in a certain area during a short period of time, the corresponding apparent stress increases rapidly, the cumulative apparent volume remains constant or has a slow growth, and the deformation of the surrounding rock mass will be small; when the apparent stress drops suddenly and the cumulative apparent volume increases dramatically, the deformation of the surrounding rock mass will grow rapidly. Consequently, the characteristics of "the accumulation of MS events in a short time, a sudden drop of apparent stress and a rapid increase of cumulative apparent volume" in the study area of interest can be used as an index of the deformation early warning of the surrounding rock masses of underground caverns.

Conclusions

The real-time on-line monitoring, analysis, and evaluation of the damage to the surrounding rock masses of underground caverns subjected to excavation were realized after the installation of the MS monitoring system at the Lianghekou hydropower station. The following conclusions were drawn.

First, MS activity is closely related to construction disturbances and the spatial structures of caverns. During the monitoring period, two aggregated regions "I" and "II" of MS events were attributed to the continuous excavations of 5# and 6# omnibus bar caves and the formation of corresponding crossover working surfaces.

Second, there is an obvious evolution regularity of the spatiotemporal migration of MS events due to the construction disturbances in the underground caverns. The expansion and migration of the active microfracture regions of the surrounding rock mass can be dynamically identified in real time and the degree and extent of the damage to the surrounding rocks subject to excavation can be delineated. Thus, the underground caverns excavation-induced security risk can be effectively avoided or reduced.

Finally, the characteristics of "the accumulation of MS events over a short time, a sudden drop of apparent stress and a rapid increase of cumulative apparent volume" observed in underground caverns can be used as an index of the deformation early warning of the surrounding rock masses.

References

Baria R, Michelet S, Baumgärtner J, Dyer B, Nicholls J, Hettkamp T, Teza D, Soma N, Asanuma H, Garnish J, Megel T (2005) Creation and mapping of 5000 m deep HDR/HFR reservoir to produce electricity. In: Proceedings of the World Geothermal Congress, Antalya, Turkey, 24–29 April 2005, paper 1627, 8pp

Boatwright J, Fletcher JB (1984) The partition of radiated energy between P and S waves. Bull Seismol Soc Am 74(2):361–376

Cai M, Kaiser PK, Martin CD (1998) A tensile model for the interpretation of microseismic events near underground openings. Pure Appl Geophys 153:67–92

Cai M, Kaiser PK, Martin CD (2001) Quantification of rock mass damage in underground excavations from microseismic event monitoring. Int J Rock Mech Min Sci 38:1135–1145

Cao AY, Dou LM, Wang CB, Yao XX, Dong JY, Gu Y (2016) Microseismic precursory characteristics of rock burst hazard in mining areas near a large residual coal pillar: a case study from Xuzhuang coal mine, Xuzhou, China. Rock Mech Rock Eng 49: 4407–4422

Cichowicz A, Green RWE, Van Zyl Brink A, Grobler P, Mountfort PI (1988) The space and time variation of micro-event parameters occurring in front of an active stope. Proceeding of the 2nd Symposium on Rockbursts and Seismicity in Mines. In: Fairhurst C (Eds.) Minneapolis. Rotterdam, A.A. Balkema, pp. 213–222

Dai F, Li B, Xu NW, Fan YL, Xu J, Liu J (2016a) Microseismic characteristic analysis of underground powerhouse at Baihetan hydropower station subjected to excavation. Chin J Rock Mech Eng 35(4): 692–703 (in Chinese)

Dai F, Li B, Xu NW, Fan YL, Zhang CQ (2016b) Deformation forecasting and stability analysis of large-scale underground powerhouse caverns from microseismic monitoring. Int J Rock Mech Min Sci 86:269–281

Dai F, Li B, Xu NW, Meng GT, Wu JY, Fan YL (2017) Microseismic monitoring of the left bank slope at the Baihetan hydropower station, China. Rock Mech Rock Eng 50:225–232

Dong LJ, Wesseloo J, Potvin Y, Li XB (2016) Discriminant models of blasts and seismic events in mine seismology. Int J Rock Mech Min Sci 86:282–291

Dong LJ, Sun DY, Li XB, Ma J, Zhang LY, Tong XJ (2018a) Interval non-probabilistic reliability of surrounding jointed rockmass considering microseismic loads in mining tunnels. Tunn Undergr Sp Tech 81: 326–335

Dong LJ, Zou W, Li XB, Shu WW, Wang ZW (2018b) Collaborative localization method using analytical and iterative solutions for microseismic/acoustic emission sources in the rockmass structure for underground mining. Eng Fract Mech 210:95–112. https://doi.org/10.1016/j.engfracmech.2018.01.032

Duplancic P (2002) Characterisation of caving mechanisms through analysis of stress and seismicity. Unpublished PhD thesis, University of Western Australia, Perth, Australia, 157p

Feng GL, Feng XT, Chen BR, Xiao YX (2015a) Microseismic sequences associated with rockbursts in the tunnels of the Jinping II hydropower station. Int J Rock Mech Min Sci 80:89–100

Feng GL, Feng XT, Chen BR, Xiao YX, Jiang Q (2015b) Sectional velocity model for microseismic source location in tunnels. Tunn Undergr Sp Tech 45:73–83

Feng GL, Feng XT, Chen BR, Xiao YX, Yu Y (2015c) A microseismic method for dynamic warning of rockburst development processes in tunnels. Rock Mech Rock Eng 48(5):2061–2076

Feng GL, Feng XT, Chen BR, Xiao YX, Zhao ZN (2019) Effects of structural planes on the microseismicity associated with rockburst development processes in deep tunnels of the Jinping-II Hydropower Station, China. Tunn Undergr Sp Tech 84:273–280

Ge MC (2005) Efficient mine microseismic monitoring. Int J Coal Geol 64:44–56

Gibowicz SJ, Young RP, Talebi S, Rawlence DJ (1991) Source parameters of seismic events at the underground research laboratory in Manitoba, Canada: scaling relations for events with moment magnitude smaller than -2. Bull Seismol Soc Am 81(4):1157–1182

Hirata A, Kameoka Y, Hirano T (2007) Safety management based on detection of possible rock bursts by AE monitoring during tunnel excavation. Rock Mech Rock Eng 40(6):563–576

Hoek E, Martin CD (2014) Fracture initiation and propagation in intact rock–a review. J Rock Mech Geotech Eng 6:287–300

Hou DQ, Yang XT, Su JD, Liu WD, Zhang CA (2016) Special report on surrounding rock mass stability and design and construction of excavation and support of underground powerhouse cavern group during the construction period in the Lianghekou hydropower station along Yalongjiang River, Sichuan Province. HydroChina Chengdu Engineering Corporation, Chengdu, p 199 (in Chinese)

Hudyma M, Potvin YH (2010) An engineering approach to seismic risk management in hardrock mines. Rock Mech Rock Eng 43(6):891–906

Li Y, Zhu WS, Fu JW, Guo YH, Qi YP (2014) A damage rheology model applied to analysis of splitting failure in underground caverns of Jinping I hydropower station. Int J Rock Mech Min Sci 71:224–234

Li A, Dai F, Xu NW, Gu GK, Liu K, Li B (2017) Failure mechanism and mode of surrounding rock of underground powerhouse at the right bank of Wudongde hydropower station subjected to excavation. Chin J Rock Mech Eng 36(4):781–793

Lu CP, Liu GJ, Liu Y, Zhang N, Xue JH, Zhang L (2015) Microseismic multi-parameter characteristics of rockburst hazard induced by hard roof fall and high stress concentration. Int J Rock Mech Min Sci 76: 18–32

Lynch RA, Wuite R, Smith BS, Cichowicz A (2005) Micro-seismic monitoring of open pit slopes. Proceeding of the 6th Symposium on Rockbursts and Seismicity in Mines. In: Potvin Y, Hudyma M. (Eds.), ACG, Perth, pp. 581–592

Ma K, Tang CA, Wang LX, Tang DH, Zhuang DY, Zhang QB, Zhao J (2016) Stability analysis of underground oil storage caverns by an integrated numerical and microseismic monitoring approach. Tunn Undergr Sp Tech 54:81–91

Ma K, Tang CA, Liang ZZ, Zhuang DY, Zhang QB (2017) Stability analysis and reinforcement evaluation of high-steep rock slope by microseismic monitoring. Eng Geol 218:22–38

Martin CD, Chandler NA (1994) The progressive fracture of Lac du bonnet granite. Int J Rock Mech Min Sci Geomech Abstr 31(6): 643–659

Song SW, Feng XM, Liao CG, Cai DW, Liu ZX, Yang YH (2016) Measures for controlling large deformations of underground caverns under high in-situ stress condition–a case study of Jinping I hydropower station. J Rock Mech Geotech Eng 8:605–618

Tang CA, Wang JM, Zhang JJ (2011) Preliminary engineering appliction of microseismic monitoring technique to rockburst prediction in tunneling of Jinping II project. J Rock Mech Geotech Eng 2(3): 193–208

Tang CA, Li LC, Xu NW, Ma K (2015) Microseismic monitoring and numerical simulation on the stability of high-steep rock slopes in hydropower engineering. J Rock Mech Geotech Eng 7:493–508

Tezuka K, Niitsuma H (2000) Stress estimated using microseismic clusters and its relationship to the fracture system of the Hijiori hot dry rock reservoir. Eng Geol 56:47–62

Trifu CI, Shumila V (2010) Microseismic monitoring of a controlled collapse in Field II at Ocnele Mari, Romania. Pure Appl Geophys 167:27–42

Urbancic TI, Trifu CI (2000) Recent advances in seismic monitoring technology at Canadian mines. J Appl Geophys 45:225–237

Urbancic TI, Young RP, Bird S, Bawden W (1992) Microseismic source parameters and their use in characterizing rock mass behaviour: considerations from Strathcona mine. In Proceedings of 94th Annual General Meeting of the CIM: Rock Mechanics and strata control sessions, Montreal, 26–30 April 1992, pp. 36–47

Wang CL (2014) Identification of early-warning key point for rockmass instability using acoustic emission/microseismic activity monitoring. Int J Rock Mech Min Sci 71:171–175

Wang HL, Ge MC (2008) Acoustic emission/microseismic source location analysis for a limestone mine exhibiting high horizontal stresses. Int J Rock Mech Min Sci 45:720–728

Xu NW, Tang CA, Li LC, Zhou Z, Sha C, Liang ZZ, Yang JY (2011) Microseismic monitoring and stability analysis of the left bank slope in Jinping first stage hydropower station in southwestern China. Int J Rock Mech Min Sci 48:950–963

Xu NW, Dai F, Liang ZZ, Zhou Z, Sha C, Tang CA (2014) The dynamic evaluation of rock slope stability considering the effects of microseismic damage. Rock Mech Rock Eng 47:621–642

Xu NW, Li TB, Dai F, Li B, Zhu YG, Yang DS (2015) Microseismic monitoring and stability evaluation for the large scale underground caverns at the Houziyan hydropower station in Southwest China. Eng Geol 188:48–67

Xu NW, Li TB, Dai F, Zhang R, Tang CA, Tang LX (2016) Microseismic monitoring of strainburst activities in deep tunnels at the Jinping II hydropower station, China. Rock Mech Rock Eng 49:981–1000

Xu NW, Dai F, Li B, Zhu YG, Zhao T, Yang DS (2017) Comprehensive evaluation of excavation-damaged zones in the deep underground caverns of the Houziyan hydropower station, Southwest China. Bull Eng Geol Environ 76:275–293

Young RP, Collins DS, Reyes-Montes JM, Baker C (2004) Quantification and interpretation of seismicity. Int J Rock Mech Min Sci 41:1317–1327

Zhang MT (1987) Instability theory and mathematical model for coal/rock bursts. Chin J Rock Mech Eng 6(3):197–204 (in Chinese)

Zhang BH, Deng JH, Gao MZ, Zhou ZH, Wu JC, Wu SH (2012) Safety evaluation research based on microseismic monitoring in underground powerhouse of hydropower station. Chin J Rock Mech Eng 31(5):937–944

Zhang PH, Yang TH, Yu QL, Xu T, Zhu WC, Liu HL, Zhou JR, Zhao YC (2015) Microseismicity induced by fault activation during the fracture process of a crown pillar. Rock Mech Rock Eng 48:1673–1682

Zhang PH, Yang TH, Yu QL, Xu T, Shi WH, Li SC (2016) Study of a seepage channel formation using the combination of microseismic monitoring technique and numerical method in Zhangmatun iron mine. Rock Mech Rock Eng 49:3699–3708